Theor Chem Acc (2014) 133:1565
DOI 10.1007/s00214-014-1565-7

REGULAR ARTICLE

NO adsorption and transformation on the BaO surfaces from density functional theory calculations

Nai-Xia Lu · Jing-Cong Tao · Xin Xu

Received: 31 May 2014 / Accepted: 8 August 2014 / Published online: 5 September 2014

Abstract Density functional theory combined with embedded cluster model calculations have been used to investigate the NO adsorption and transformation reactions on the BaO(100) surfaces. NO is found to adsorb on the anion sites to form a NO_2^{2-} species, which can then couple with another NO to form a $N_2O_3^{2-}$ species. These surface species provide an alternative explanation for the infrared bands that were used to be assigned to the nitrite/nitrate and hyponitrite species. The calculations suggest a large intrinsic barrier for the transformation from $N_2O_3^{2-}$ to $N_2O_2^{2-}$. The latter species acts as a chemisorbed N_2O, which is envisioned as a key intermediate for further NO reduction. The present study provides a detailed description at the molecular level for the NO/BaO(100) system, which shed some light on the NO_x storage–reduction systems, as well as NO direct decomposition.

Keywords NO_x storage and reduction · BaO · NO_x trap · Lean-burn · DFT · Vibrational properties

Dedicated to Professor Guosen Yan and published as part of the special collection of articles celebrating his 85th birthday.

Electronic supplementary material The online version of this article (doi:10.1007/s00214-014-1565-7) contains supplementary material, which is available to authorized users.

N.-X. Lu · J.-C. Tao (✉)
Laiwu Vocational and Technical College, Laiwu 271100, China
e-mail: jingcongtao@gmail.com

X. Xu (✉)
Shanghai Key Laboratory of Molecular Catalysis and Innovative Materials, MOE Laboratory for Computational Physical Science, Department of Chemistry, Fudan University, Shanghai 200433, China
e-mail: xxchem@fudan.edu.cn

1 Introduction

The need for fuel economy and consequently a reduction in CO_2 emissions for environmental protection has brought about the lean-burn engine technology with high air/fuel ratio for motor vehicles. In such a circumstance, however, the conventional three-way catalysts (TWC) in removing engine exhausts, notably CO, hydrocarbons (HC) and nitrogen oxides (NO_x), are no longer effective in removal of NO_x. One promising solution to this problem is to use the so-called NO_x storage–reduction (NSR) catalyst [1–5]. The concept of NSR is that NO_x is first stored under the lean condition over the catalyst, which is regenerated during the short periods of rich conditions, where NO_x is released and subsequently reduced with HC, H_2 and CO to form N_2, H_2O and CO_2 [6–8]. A typical NSR catalyst consists of noble metals (generally Pt) for the purposes of NO oxidation/reduction, and materials with Lewis basicity (notably a metal oxide like BaO) for the purposes of NO_x storage, which are dispersed on a high surface area support like γ–Al_2O_3 [1, 6–8]. To further improve the performance of the catalysts in regard of NO_x storage ability, temperature stability, regeneration times, and sulfur resistance, a good knowledge about the storage and transformation mechanisms is vital.

Despite the fact that huge efforts have been dedicated to kinetic measurements and spectroscopic characterizations [e.g., 1–31], certain key aspects concerning the mechanistic features of the NSR processes remain elusive, such that no clear understanding of this catalytic system has emerged [1, 5]. The difficulty arises not only from the variations of the operation conditions, but also from the complexity of both the reactant gas mixture (i.e., NO, NO_2, O_2, H_2O, CO_2, etc.) and the catalyst material (e.g., Pt/Ba/γ–Al_2O_3) with the abundance of the different adsorption and reaction sites. To

build a comprehensive understanding of the mechanism and to set up a predictive kinetic model concerning how different reactant gases adsorb, react and even compete against each other for active sites, and how different components of catalyst materials interplay to enhance or depress the reaction activity, model catalysts and model reactant gases have to be employed to individually probe the adsorption and chemistry on different sites [10–14, 17–28]. Along this line, the present work focuses only on NO, which is the main form of NO_x in exhaust gas, adsorbed on and reacted with BaO, which is the primary storage material, with embedded cluster model calculations using density functional theory. The results shall be best compared with the experiments concerning NO adsorption and reactions on BaO surfaces by surface chemistry approaches [12, 13, 15, 23, 26].

In a NSR catalytic system, it is generally believed that NO is first oxidized to NO_2 on noble metal sites,

$$NO + \frac{1}{2}O_2 \overset{Pt}{\rightleftharpoons} NO_2 \tag{1}$$

which is then stored on BaO as nitrites (NO_2^-) and nitrates (NO_3^-) [6–11]. However, such a conversion was shown to be kinetically limited at lower temperature and thermodynamically limited at higher temperature [1, 11]. For example, Muncrief et al. [11] reported a <30 % steady-state NO to NO_2 conversion at temperatures below 250 °C and above 450 °C, with a maximum conversion of 60 % around 350 °C on a $Pt/Ba/Al_2O_3$ catalyst for a gas feed of 500 ppm NO and 5 % O_2 flowing at 200 cm^3/min. Hence, understanding the NO adsorption and transformations is an important issue in unraveling the NO_x storage mechanism.

In experiments, the ad-species of NO exposure on barium-containing catalysts is complicated and controversial. The NO storage on monolith experiments showed that negligible conversion of NO to NO_2 occurred with the Pt-free catalyst, and catalysts with >1 % Pt loading had significantly improved the trapping efficiencies [21]. These experiments suggested the importance of a Pt–Ba couple and associated spillover processes that enhanced the storage [10, 18, 21]. Temperature-programmed desorption (TPD) experiments were carried by Mahzoul et al. [19], which also confirmed the role of platinum. Nevertheless, they showed that NO storage was already significant even if no oxygen was present in the gas phase and even in the absence of platinum [19]. Hence, their experiments suggested that BaO alone is reactive toward pure NO. The X-ray photoelectron spectroscopy (XPS) has been used to characterize the ad-species of NO on a 15–20 Å BaO film deposited on the aluminum substrate [12], where the influence of the substrate was actually minimized. The nitrogen and oxygen core level spectra acquired following NO exposure strongly suggested that new ad-species had formed, which were primarily ascribed as a nitrite-like species (NO_2^-), accompanied by the formation of a small amount of nitrate-like ad-species (NO_3^-) [12]. These results were, however, not supported by a later XPS and TPD investigation on BaO layers deposited on Cu(111) surfaces [23], which concluded that BaO itself did not readily trap NO. A systematic study of the $Pt/Ba/Al_2O_3$ system was performed by Prinetto et al. [13]. The evolutions of the surface species were monitored with FT-IR where $Pt/Ba/Al_2O_3$, Pt/Al_2O_3, BaO/Al_2O_3, and Al_2O_3 were exposed independently to NO or NO_2 in O_2. A couple of sharp bands at 1,375 and 1,310 cm^{-1}, a complex absorption at 1,050–950 cm^{-1} with maximum at 1,025 cm^{-1} and bands of minor intensity at 1,600, 1,470, and 1,220–1,180 cm^{-1} were observed upon NO adsorption on either Ba/Al_2O_3 or $Pt/Ba/Al_2O_3$ [13]. Regardless of the presence of platinum or not, there was little difference on the IR spectra for these two systems [13]. Based on these results, the formation of nitrites (NO_2^-), nitrates (NO_3^-), and hyponitrite ($N_2O_2^{2-}$) species was assumed, and a mechanism was postulated [13]

$$2\,NO + O^{2-}_{(s)} \longrightarrow NO^- + NO^-_{2(s)} \tag{2}$$

$$4\,NO + 2\,O^{2-}_{(s)} \longrightarrow 3\;NO^-_{(s)} + NO^-_{3(s)} \tag{3}$$

$$2\,NO^-_{(s)} \longrightarrow N_2O^{2-}_{2(s)} \tag{4}$$

However, it should be noted that these seemingly simple steps are actually sum of several elementary reaction steps, which already includes some uncertainties. For example, the suggested formation of the hyponitrite species involves coupling of two negative species (NO^-), which is suspicious due to the large electrostatic repulsion.

In NSR, conversion to N_2 is also thought to occur over noble metal sites, which generally involves NO dissociation to form atomic N and O on platinum, where N_2O was found to be an important product at lower temperature when the NO coverage is higher [1, 11, 18, 21, 29]. Although the primary focus of this study is the NSR system, direct decomposition of NO is also of interest. In fact, decomposition of NO over metal oxides in no presence of noble metals has been actively studied [31–35]. For example, Lunsford and co-workers have studied the BaO supported MgO systems using in situ Raman spectroscopy. This system was claimed to be particularly active for NO decomposition at Ba loadings of 11 mol% or greater, where a nitro species was assumed to be an intermediate in the catalytic cycle [31]. Recently, NO direct decomposition on the BaO/Y_2O_3 catalyst was reported by Ishihara et al. [35]. N_2O, nitrite and nitrate species were supposed to form based on IR spectra. Thus, the disproportional reactions of NO were suggested to occur [35]:

$$3\,NO \longrightarrow N_2 + NO_3 \quad (5)$$

$$3\,NO \longrightarrow N_2O + NO_2 \quad (6)$$

Clearly, Eqs. 5 and 6 do not refer to elementary steps and the mechanistic details remain to be clarified.

Identification of reaction pathways and intermediates by means of experiments represents a great challenge, while theoretical calculations can help to gain a more clear-cut answer for a given model system. So far, only a few theoretical calculations, based on either periodic-slab models [36, 37] or cluster models [38–40] have been carried out to investigate the interaction of NO with the BaO surfaces. It was generally agreed that NO adsorbs on the oxygen anion sites to form a NO_2^{2-} species [38, 39]. However, the subsequent reactions of the surface species and the possible reaction paths that lead to the formation of the possible hyponitrite ($N_2O_2^{2-}$) species and the release of N_2O have not yet been explored.

Thermodynamics for NO decomposition on MgO has been studied using cluster model calculations, where no transition states have been characterized [41]. A $N_2O_3^{2-}$ species was proposed to be an important intermediate in the NO decomposition process [41]. Unlike the neutral N_2O_2 dimer, it was noticed that anionic dimeric species such as $N_2O_2^{-}$ and $N_2O_2^{2-}$ present a much shorter N–N bond, typical of the N–N double bond [42, 43]. Therefore, charge transfer from the adsorption site to the ad-species was essential to activate the adsorbed precursors for the production of molecular N_2O [42]. On MgO, the lattice sites were found to interact with NO very weakly [41], while chemisorbed species was formed only at low-coordination anions (steps, edges, or corners) or oxygen vacancies [42, 43]. As it is well known that the surface basicity of the cubic alkaline earth oxides (MgO, CaO, SrO, and BaO) increases going down the series as a result of the reduction of the Madelung potential with the crystal lattice expansion [44], the more basic anions on the BaO surfaces are expected to facilitate the NO adsorption and subsequent reactions.

The present theoretical study deals with NO adsorption and transformation on BaO surfaces. It aims, on the one side, at providing a detailed understanding of NO and BaO interactions at the molecular level, and on the other side, at complementing the available experimental work to gain, in particular, a better assignment of the species observed in the IR spectra.

2 Computational details

Density functional theory (DFT) calculations were carried out using the gradient-corrected Becke three-parameter hybrid exchange functional [45–49] in combination with the correlation functional of Lee, Yang, and Parr [50] (B3LYP). Recently, the inter-conversion between NO_2 and N_2O_4 has been studied using the B3LYP functional and several ab initio methods (MP2, CCSD(T), etc.). The results indicated that the B3LYP functional led to good energetics for these conversions [51].

An embedded cluster model approach was adopted to describe the BaO(100) surface as well as the low-coordination surface sties. A $Ba_{16}O_{16}$ cluster was chosen to represent the BaO(100) terrace sites (O_{5c}), while $Ba_{12}O_{12}$ and $Ba_{10}O_{10}$ were used as models for the four-coordinated edge sites (O_{4c}), and the three-coordinated corner sites (O_{3c}), respectively (see Fig. 1). These cluster models were constructed in fulfillment of some general requirements, namely the neutrality principle, the stoichiometry principle, and the coordination principle [52–56]. All these clusters were embedded in a large array of ±2 point charges (PCs), which were aimed to reproduce the Madelung potential at the adsorption sites. A Ba–O lattice distance of 2.76 Å was assumed [57]. To avoid the artificial polarization of the O^{2-} anions at the cluster border induced by the PCs, the positive PCs at the interface were replaced by the total ion effective core potentials (TIPs) [58–60] to ensure a proper description of the Pauli repulsion. No basis functions were associated with the TIPs. The Ba atoms in the clusters were also treated with the effective core potentials (ECPs) originally developed by Hay and Wadt [61]. These were the small core ECPs with the contraction scheme generally known as LANL2DZ. The O and N atoms were described with a 6–31+G* basis set [62, 63].

Geometry optimizations were performed by means of analytical gradients with no symmetry constraints. The adsorbed NO molecules and atoms in clusters which were not in direct contact with the TIPs were included in the geometry optimization. Vibration frequencies were computed by determining the second derivatives of the total energy with respect to the internal coordinates. No scaling factors were applied when comparing the calculated frequencies with the experimental ones.

The adsorption enthalpy changes at room temperature were calculated using the formula:

$$\Delta H_{ad} = H_{tot}^{clus+ad} - H_{tot}^{clus} - H_{tot}^{ad} \quad (7)$$

where $H_{tot}^{clus+ad}$, H_{tot}^{clus}, and H_{tot}^{ad} refer to the total enthalpy of the full system (BaO cluster + adsorbate), the enthalpy of the bare BaO cluster, and the enthalpy of the gas-phase molecules, respectively. According to this definition, $\Delta H_{ad} < 0$ stands for an exothermic adsorption.

Cluster models have generally been recognized as a useful tool to facilitate analysis and to be able to treat the neutral (e.g., NO and NO dimer) and charged adsorbates (e.g., nitrite and nitrate) on metal oxide surfaces even-handedly [64]. Previously, the same methodology has been used to study the O_2 dissociation mechanisms over the BaO(100)

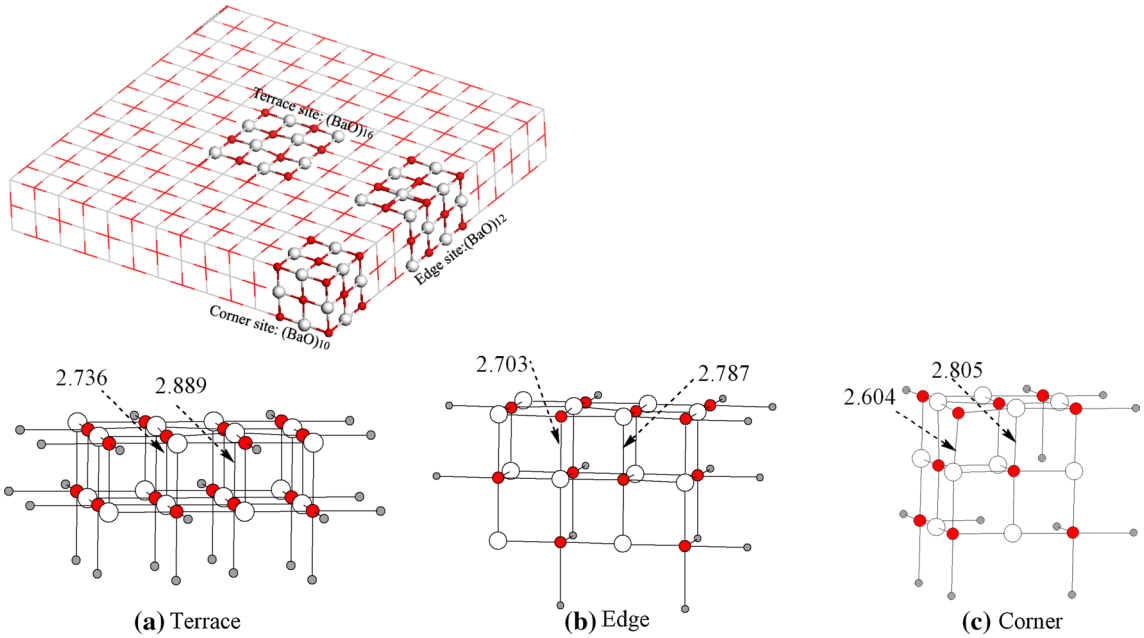

Fig. 1 Cluster models used in the present work: **a** $(BaO)_{16}$ for terrace sites, **b** $(BaO)_{12}$ for edge sites, and **c** $(BaO)_{10}$ for corner sites. *Red spheres* stand for O^{2-}, while *large white spheres* for Ba^{2+}. *Small gray spheres* refer to the point charges (PCs) that are in close contact with O^{2-} in the clusters as described by the total ion effective core potentials (TIPs). The rest of PCs are not shown

surface [65]. Other related studies, in particular, regarding the cluster size and embedding method [64–67], have well documented the validity of the present methodology [64–77].

All calculations were performed with the Gaussian 03 suite of program [62].

3 Results and discussion

3.1 One NO adsorption

On the terrace sites of the BaO(100) surfaces, our calculations predict that NO binds, with the N-down orientation, quite strongly to the O_{5c} anion sites [see Fig. 2(**1**)]. The adsorption energy is calculated to be $\Delta H_{ad} = -28.4$ kcal/mol (see Table 1). Mulliken analysis shows that the unpaired spin density is almost entirely localized on the adsorbed NO (0.95, as shown in Table S1 in the supporting information, SI). Upon adsorption, the NO moiety is negatively charged (−0.89), such that partial charge is transferred from the surface anion (O_s) to the antibonding π^* orbital of the adsorbed NO, resulting in an elongation of the N–O bond length from 1.158 Å in the gas phase to 1.291 Å on the surfaces. As a relatively short O_s–N bond (1.516 Å) is formed, the adsorption of NO on the O_s site can be formally regarded as the formation of a NO_2^{2-} species:

$$NO + O^{2-}_{(s)} \longrightarrow NO^{2-}_{2\,(s)} \quad (8)$$

This was first postulated by Lunsford based on the results of the electron paramagnetic resonance (EPR) technique on MgO [78] and was later supported by the observation on CaO [79]. Certainly, NO_2^{2-} is unstable as an isolated species. It is stabilized on the surfaces by the Madelung potential.

As expected, the reactivity on the low-coordination sites for such an adsorption is much higher than that on the terrace sites due to the increased basicity of O_s [44]. For instance, The NO adsorption energies on the O_{4c} edge sites, or the O_{3c} corner sites, are calculated to be −38.8 and −46.1 kcal/mol, respectively (Table 1). The stronger interactions are also reflected in the shorter O_s–N distances of 1.461 Å, and 1.423 Å on the O_{4c} and O_{3c} sites, respectively (Table S1). Spin densities (0.92) are nearly localized on the NO moieties which carrier more negative charges (−0.98), as compared to that on the terrace site, in accord with the increased adsorption energies.

Previously, a detailed comparison between the slab model and the embedded cluster model has been carried out in the study of the O_2 dissociation mechanisms over the BaO(100) surface [65]. A general agreement on the reaction trend was observed with these two methods. The calculations for NO adsorption are also generally in agreement with previous slab model [36, 37] and cluster model [38, 39] calculations. For example, with cluster models [38], Pacchioni et al. calculated the adsorption energies for NO on the O_{5c} terrace and O_{4c} step sites to be −18.4, and −38.0 kcal/mol, respectively. It is interesting to note that

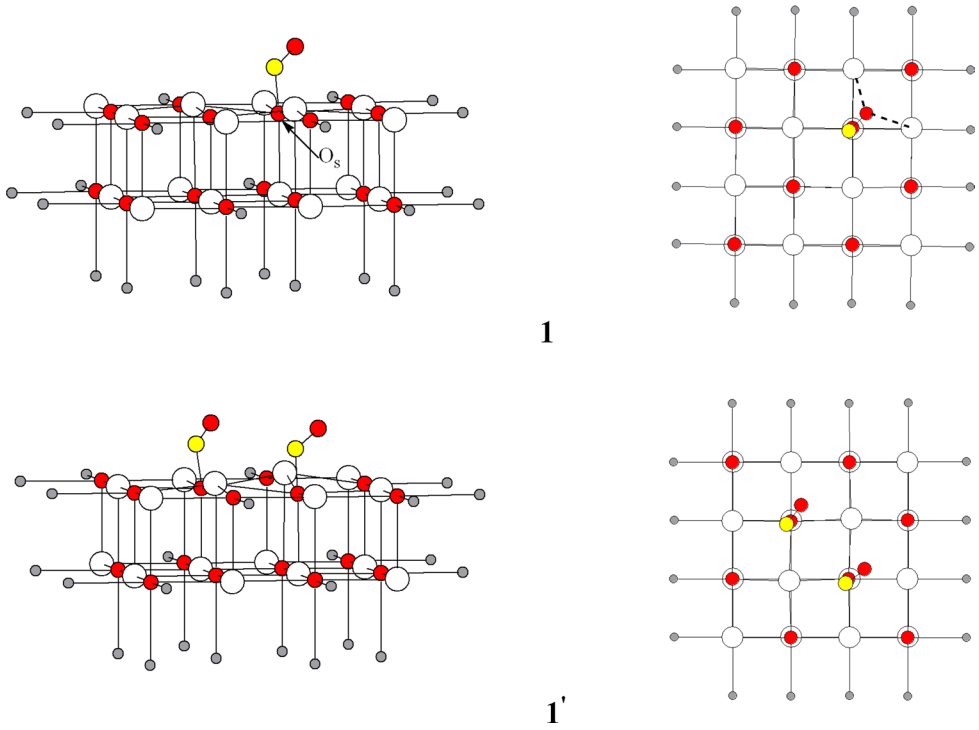

Fig. 2 Optimized structures. **1** for one NO molecule adsorbed on an O_{5c} anion site at the terrace of BaO (*left*, *side view*; *right*, *top view*); **1′** for two NO molecules adsorbed on two neighboring O_{5c} anion sites at the terrace of BaO (*left*, *side view*; *right*, *top view*). *Color codes*: *yellow spheres* for N, *red spheres* for O, *large white spheres* for Ba and *small gray spheres* for TIPs. Geometric details are given in Table S1 in supporting information (SI)

Table 1 The adsorption energies ΔH_{ad} (kcal/mol)[a] for one and two NO (the triplet state) adsorbed on the surface anion sites (O_s) of BaO[b]

Adsorption geometry	Terrace	Edge	Corner
One NO adsorption (**1**)	−28.4	−38.8	−46.1
Two NO adsorption (**1′**)	−58.1	−66.9	−70.2

a The adsorption energies are calculated according to $\Delta H_{ad} = H_{tot}^{clus+n*NO} - H_{tot}^{clus} - n*H_{tot}^{NO}$, where $n = 1, 2$

b The corresponding adsorption configurations are illustrated in Fig. 2

although a similar stability on the O_{4c} sites was obtained, their adsorption energies on the O_{5c} terrace sites were predicted to be less stable by ~10 kcal/mol than ours. The discrepancy is probably due to the difference in cluster size and the allowed surface relaxation. For adsorption on the terrace sites, besides the adsorbed NO molecule, the four-center ions of the $(BaO)_{16}$ cluster have been included in the present geometry optimization, while in the previous work [38], only the central O atom of the $(BaO)_9$ cluster was free to relax. The contribution to the adsorption energy associated with the surface relaxation can be significant. In our case, if only the central oxide anion was involved in the geometry optimization, the adsorption energy was found to decrease by ~4 kcal/mol. On the other hand, the effect of surface relaxation is usually well considered in the slab model calculations. For instance, the binding energies for NO adsorption on the BaO(100) surface were reported to be about −34 kcal/mol at a coverage of 0.25 [36, 37].

The frequency analysis shows that the N–O stretch band appears at 1,317 cm^{-1} on the BaO terrace sites (Table 3), which may be compared to, for example, the observed frequency (1,300 cm^{-1}) for NO exposure on the BaO/Y_2O_3 catalyst [35]. With the decreasing of the coordination number of the adsorption sites, the N–O stretch band experiences a red shift to 1,241 cm^{-1} on the O_{4c} edge sites, and to 1,096 cm^{-1} on the O_{3c} corner sites, respectively. Therefore, we are inclined to associate the NO_2^{2-} species with the broad band at 1,206 cm^{-1} that was observed by Sedlmair et al. [15] in their IR experiments, although they tentatively assigned this band to the bridged bidentate nitrites.

3.2 Two NO adsorption

A key theoretical concept in understanding the interaction between NO_x and the basic metal oxides is a pairwise, cooperative adsorption mechanism [36]:

$$M^{2+} - NO_x + NO_x - O^{2-} \longrightarrow M^{2+} - (NO_x)^{\delta-}/(NO_x)^{\delta+} - O^{2-} \quad (9)$$

where NO_x molecules, adsorbed on metal cation sites, and oxygen anion sites, respectively, accept and donate electrons. Such a unique ability of NO_x is a consequence of their high electron affinity and low ionization energy. The electron transfer between two NO_x adsorbates in close proximity through the substrate results in a substantial increase of the adsorption energies for the pair in comparison with two individual adsorbates in isolation. This effect

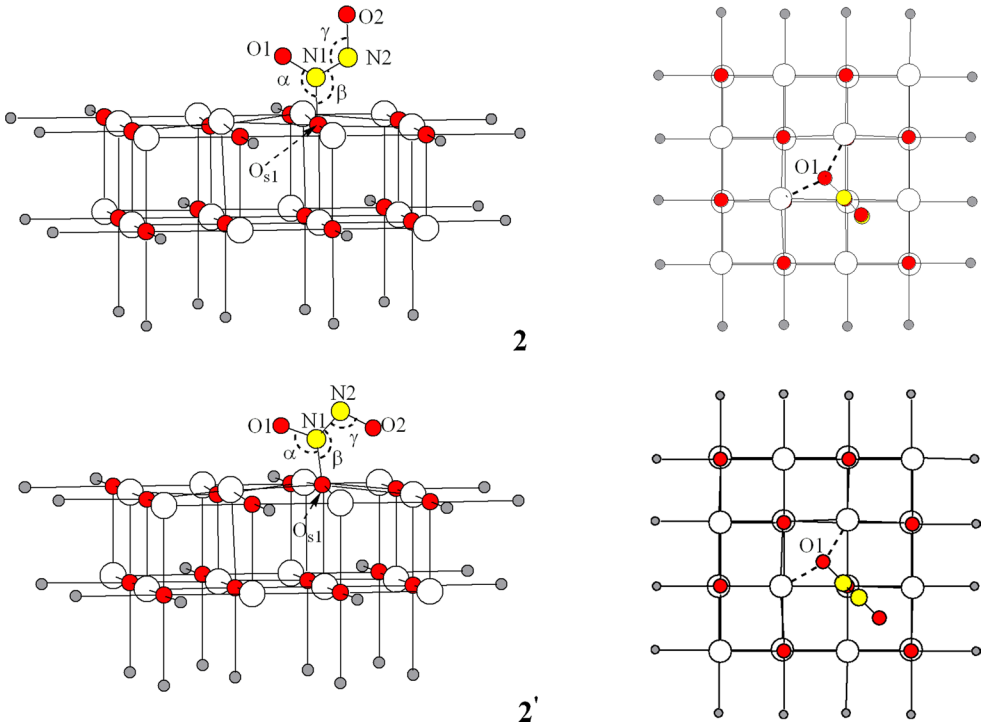

Fig. 3 Optimized structures for NO dimer adsorbed on an O_{5c} anion site at the terrace of BaO, forming *cis*-$N_2O_3^{2-}$ (**2**) and *trans*-$N_2O_3^{2-}$(**2′**) (*left*, *side view*; *right*, *top view*). *Color codes*: *yellow spheres* for N, *red spheres* for O, *large white spheres* for Ba and *small gray spheres* for TIPs. Geometric details are given in Table S1 in supporting information (SI)

has been observed for the (NO, NO_2), (NO_2, NO_2), (NO_2, NO_3) pairs, but not for the (NO, NO) pair [36].

Adsorption of two NO molecules on the BaO surfaces is studied in the present work, where both NO molecules are found to adsorb on the O anion sites. The adsorption configuration on two adjacent O_{5c} sites is shown in Fig. 2 (**1′**), while geometries for some other configurations may be found in Table S1 in SI. As shown in Table 1, the adsorption energy per molecule on a terrace site is −29.05 kcal/mol, no matter the electronic state is set to either a triplet or an open-shell singlet. This energy actually compares well with the adsorption energy of the singly adsorbed molecule, indicating that there is little enhanced pairwise cooperative effect. The same is true if two NO molecules are adsorbed on a pair of O_{5c} and O_{4c} sites. Interestingly, if adsorption occurs on a pair of (O_{5c}, O_{3c}) sites, a repulsion of 3.8 kcal/mol is encountered (see Table 1).

The coverage dependence of NO adsorption on the BaO(100) surface was reported with the slab model calculations [37]. The results showed that the binding strength of NO on the anion sites almost linearly decreased with the increasing coverage from 34.6 kcal/mol at $\theta = 0.125$–23.1 kcal/mol at $\theta = 0.5$. Therefore, as indicated by the present cluster model calculations and the previous slab model calculations [37], some other adsorption configurations containing NO dimer may be more favorable at higher NO coverage.

As described above, the isolated NO binds strongly on the O_s sites to form a NO_2^{2-} species even on the terrace sites of BaO. As both the NO_2^{2-} species and the free NO molecule carry one unpaired electron on the N atom, respectively, a singlet $N_2O_3^{2-}$ species would be formed by coupling the two radical-like groups (see Fig. 3):

$$NO^{2-}_{2\,(s)} + NO \longrightarrow N_2O^{2-}_{3\,(s)} \tag{10}$$

The $N_2O_3^{2-}$ complex can also be regarded as the adsorption of a NO dimer (N_2O_2) on the surface O anion site. These have been studied before on MgO [41], as well as BaO [39]. The configurations of the $N_2O_3^{2-}$ surface complexes can be assigned to *cis*-$N_2O_3^{2-}$ and *trans*-$N_2O_3^{2-}$ with respect to *cis*-N_2O_2 and *trans*-N_2O_2, respectively. The corresponding geometrical parameters are listed in Table S2 in SI. The N–N bond length is dramatically reduced from 1.96 Å for *cis*-N_2O_2 in the gas phase [42] to 1.29–1.32 Å, depending on the orientation, while the N–O bond length is drastically elongated from 1.16 Å in the gas phase [42] to 1.30–1.34 Å. Mulliken charge analysis shows that the adsorbed NO dimer on the terrace anion sites almost obtains one electron (−0.84 for the *cis* form and −0.75 for the *trans* form), which is increased to −1.0 and −1.3 for the low-coordination anion sites on the edges and corners, respectively (see Table S2 in SI). Such an electron transfer from the surface anion sites to the NO dimer reinforces the bond strength of N–N, while weakens the N–O bond simultaneously, which then triggers the direct dissociation channel from $N_2O_3^{2-}$ into N_2O as described in the next section.

Table 2 The adsorption energies ΔH_{ad} (kcal/mol)[a] for a NO dimer adsorbed on the surface anion sites (O_s) of BaO[b]

Adsorption geometry	Terrace	Edge	Corner
cis-$N_2O_3^{2-}$ (**2**)	−41.4	−58.3	−89.7
trans-$N_2O_3^{2-}$ (**2′**)	−41.0	−68.5	−89.9

[a] The adsorption energies are calculated according to $\Delta H_{ad} = H_{tot}^{clus+(NO)_2} - H_{tot}^{clus} - 2 * H_{tot}^{NO}$

[b] The corresponding adsorption configurations are illustrated in Fig. 3

The adsorption energies of the NO dimer on the terrace as well as edge and corner anion sites are summarized in Table 2. On the terrace sites, the stability of the *cis*- and *trans*-$N_2O_3^{2-}$ is similar with an exothermicity of ~41 kcal/mol with respect to two free NO molecules. On the low-coordination anion sites, the $N_2O_3^{2-}$ species are calculated to be more stable. On the edge sites, formations of the *cis*- and *trans*-$N_2O_3^{2-}$ species are exothermic by 58.3 and 68.5 kcal/mol, respectively, while on the corner sites, both *cis*- and *trans*-$N_2O_3^{2-}$ show a large stability with the adsorption energy of about −90 kcal/mol.

The formation of the stable $N_2O_3^{2-}$ species represents the N–N bond formation which should be identified by the IR spectra. Previously, the bands around 1,310 and 1,375 cm^{-1} as observed by Prinetto et al. [13] and the peak around 1,380 cm^{-1} as observed by Sedlmair et al. [15] were associated with the N–N stretching in the $N_2O_2^{2-}$ species. This is fairly reasonable if one compares them with the N–N stretching in the $Na_2N_2O_2$ salts, which appear around 1,314 and 1,419 cm^{-1} [80]. However, as listed in Table 3, our calculated N–N stretching frequencies are also around 1,354 cm^{-1} for *cis*-$N_2O_3^{2-}$ and 1,413 cm^{-1} for *trans*-$N_2O_3^{2-}$, even though the corresponding peak appears at much low region of 1,120 cm^{-1} in the $Na_2N_2O_3$ salts [80]. Hence, a band of the same nature may appear at different position on surfaces and in compounds. The present calculations offer a new insight into the assignment of the N–N stretching bands, which may indicate the formation of the $N_2O_3^{2-}$ species on the surfaces.

3.3 $N_2O_3^{2-}$ dissociation

The proposed mechanisms for NO decomposition via $N_2O_3^{2-}$ species are presented in Scheme 1. It is initialized by the formation of species **1** (NO_2^{2-}) via the adsorption of an NO molecule on the oxygen anion sites, then followed by the coupling of the second gas-phase NO to **1** to produce **2** (*cis*-$N_2O_3^{2-}$) or **2′** (*trans*-$N_2O_3^{2-}$), depending on the orientation. The dissociation of species **2** (**2′**) occurs through the cleavage of one of the N–O bonds, leading to the formation of species **3**(**3′**), which corresponds to a $N_2O_2^{2-}$ species plus a peroxide species of O_2^{2-} on the surface. A rearrangement of $N_2O_2^{2-}$ generates the lattice oxygen anion with an electrostatically adsorbed N_2O as in **4**(**4′**). The final step is envisioned as the desorption of N_2O, leaving the peroxide on the surfaces.

The transition states and intermediates in the dissociation processes on the terrace sites are presented in Figs. 4 and 5, respectively. The corresponding enthalpy changes, defined in Scheme 1, are summarized in Table 4, which are depicted in Fig. 6. The detailed geometric parameters are given in Tables S3 and S4 in SI.

Table 3 Calculated vibrational frequencies (cm^{-1}) for the adsorption species on the BaO terrace sites

The experimental IR spectra for free molecules[a] , ions in compounds[a] and the NO/BaO/Al_2O_3 system[b] are also listed for comparison

[a] Data from Ref. [63] for free molecules and ions in compounds

[b] From IR spectra for NO/BaO/Al_2O_3 at room temperature [13]

[c] Assigned to the surface $N_2O_2^{2-}$ species [13]

[d] Assigned to the surface NO_2^- species [13]

[e] Assigned to the surface NO_3^- species [13]

	ν_1 (N–N stretch)	ν_2 (N–O stretch)
Calc.		
NO adsorption (1)	–	1,317
Two NO adsorption (1′)	–	1,313 (symmetry), 1,309 (asymmetry)
cis-$N_2O_3^{2-}$ (2)	1,354	1,410
trans-$N_2O_3^{2-}$ (2′)	1,413	1,282
trans-$N_2O_2^{2-}$ (3)	1,279	1,417
cis-$N_2O_2^{2-}$ (3′)	1,380	1,241
adsorbed N_2O (4)	1,884	1,118
adsorbed N_2O (4′)	2,378	1,315
Expt.		
NO[a]	–	1,876
N_2O[a]	2,224	1,285
NO_2^- [a]	–	1,260 (asymmetry), 1,330 (sym.)
NO_3^- [a]	–	1,380 (asymmetry), 1,050 (sym.)
$N_2O_3^{2-}$[a]	1,120, 1,100	1,400, 1,380 (asymmetry NO_2), 1,280 (sym. NO_2), 980, 970
cis-$N_2O_2^{2-}$[a]	1,314	1,057 (sym.), 857 (asymmetry)
trans-$N_2O_2^{2-}$[a]	1,419	1,120 (sym.), 1,030 (asymmetry)
NO/BaO/Al_2O_3[b]	1375[c], 1310[c]	1,050–950[c], 1,220–1,180[d], 1,600[d], 1470[e]

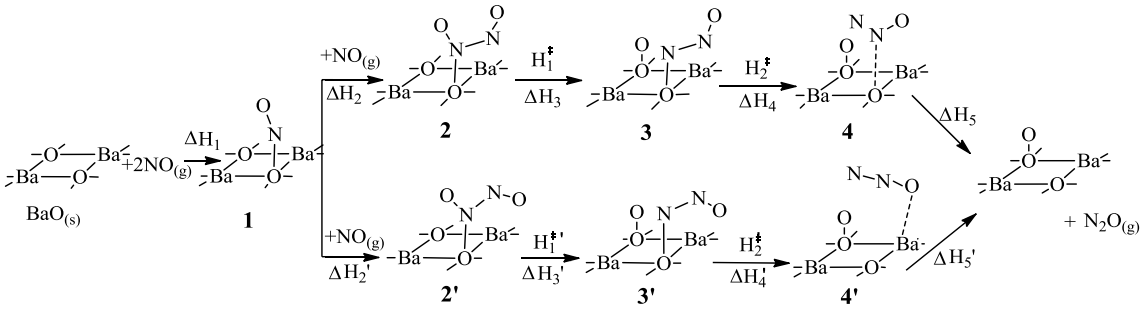

Scheme 1 The possible reaction pathways of NO decomposition on BaO (100) surfaces

We first look at the dissociation of *cis*-$N_2O_3^{2-}$ (**2**) on the terrace sites of the BaO surfaces. A transition state (**TS1** in Fig. 4) is located, which clearly indicates the cleavage of a N–O bond and the formation of an O_s–O bond. The as-formed **3** is lower lying by 12.5 kcal/mol on the terrace with respect to **2**. Notably in **3**, a surface peroxide species (O_2^{2-}) can be envisioned. This is characterized by an O_s–O bond length of 1.523 Å as shown in Table S4 in SI, which approaches to the bond length of a standard peroxo species (1.49 ± 0.02 Å, [81]). Meanwhile, a relatively short O_s–N bond with the distance of 1.46 Å is maintained, which is accompanied by a N–N bond of 1.30 Å (See Table S4). The latter compares well with the N–N distance in the standard $N_2O_2^{2-}$ species (1.27 Å [80]). We thus assign this entity as a surface $N_2O_2^{2-}$ species. It has to be noted that the transformation from the $N_2O_3^{2-}$ (**2**) species to the $N_2O_2^{2-}$ species in **3** on the terrace sites needs to surmount an intrinsic reaction barrier of 52.8 kcal/mol. Hence, it is necessary to increase the reaction temperature to facilitate the $N_2O_2^{2-}$ formation.

Thereafter, **3** experiences a geometry relaxation and leads to the formation of **4** by overcoming a reaction barrier of 25.0 kcal/mol on the terrace sites via **TS2**. The geometrical features of **TS2** (see Fig. 4 and Table S3 in SI) clearly indicate the N_2O formation with the N–N bond length of 1.18 Å and the N–O length of 1.28 Å, which is accompanied by a strongly elongated O_s–N bond (2.11 Å). In **4** on the terrace, the as-formed N_2O is found to be adsorbed on the surface anion site via the middle N atom (see Fig. 5). There is still a sizable charge transfer from O_s to N_2O (0.57 as listed in Table S4 in SI), leading to a NNO which is bent by 138°, instead of adopting a linear NNO structure as in free N_2O. We find that there is an energy cost of 10.2 kcal/mol from **3** to **4**.

Now, we look at the dissociation of *trans*-$N_2O_3^{2-}$ (**2′**) on the terrace site of the BaO surfaces. As shown in Fig. 6, the dissociation route is basically the same as that of the *cis*-$N_2O_3^{2-}$ species. The whole energetics is more favorable, as compared to the dissociation of *cis*-$N_2O_3^{2-}$ (**2**), due to a more favorable electrostatic interaction between the trans-configurations of the ad-species and the surfaces. Indeed, **TS1′** is 5.7 kcal/mol lower lying than **TS1**, while **TS2′** is 17.3 kcal/mol more stable than **TS2**. The geometry features of N_2O in **4′** are shown in Fig. 5 and Table S4 in SI. The adsorbed N_2O is nearly linear (177°), which is nearly charge neutral. Hence, one may consider the $N_2O_2^{2-}$ species in **3**(**3′**) as a chemisorbed N_2O on the surface, the N_2O moiety in **4**, in particular **4′,** shall be considered as a physisorbed species.

The energy profiles show that the dissociation of $N_2O_3^{2-}$ on the terrace sites is characterized by a large barrier encountered at **TS1**(**TS1′**) for the formation of $N_2O_2^{2-}$, followed by a small barrier at **TS2**(**TS2′**) which eventually leads to the N_2O formation. Hence, if the first barrier can be overcome, e.g., with the help of other components in the catalyst at high temperature, it is possible that NO undergoes direct dissociation over BaO as it was observed in the BaO/MgO [31] or BaO/Y_2O_3 [35] system. On the other hand, we conclude that NO initially adsorbs on BaO as NO_2^{2-} and $N_2O_3^{2-}$ at low temperature in no presence of O_2 and Pt.

We have also examined the dissociation of $N_2O_3^{2-}$ on the low-coordination sites of the BaO surfaces. The corresponding enthalpy changes are also summarized in Table 4 and depicted in Fig. 6. The detailed geometric parameters may be found in SI. Even though the intrinsic barriers to transform $N_2O_3^{2-}$ (**2** or **2′**) to $N_2O_2^{2-}$ (**3** or **3′**) remain to be high (54.8–62.1 kcal/mol), the strong basicity of the low-coordination sites is found to significantly enhance the stabilities of the $N_2O_3^{2-}$ species, which actually brings the transition states (**TS1** or **TS1′**) lower (by −3.5 to −30.0 kcal/mol) than the entrance level (**BaO + 2 NO**), rendering these dissociation processes having no apparent barriers. Therefore, the $N_2O_3^{2-}$ dissociation on the low-coordination surface sites is predicted to be easier than that on the terrace sites. In addition, the increased basicity from terrace to edge to corner sites has significantly increased the amount of the change transfer from 0.57 to 0.90 to 1.34 from the surfaces to the N_2O moiety (see Table S4 in SI), which stabilizes the bent N_2O in **4**. In fact, both **TS2** and **TS2′** are found to connect with **4** on the low-coordination sites.

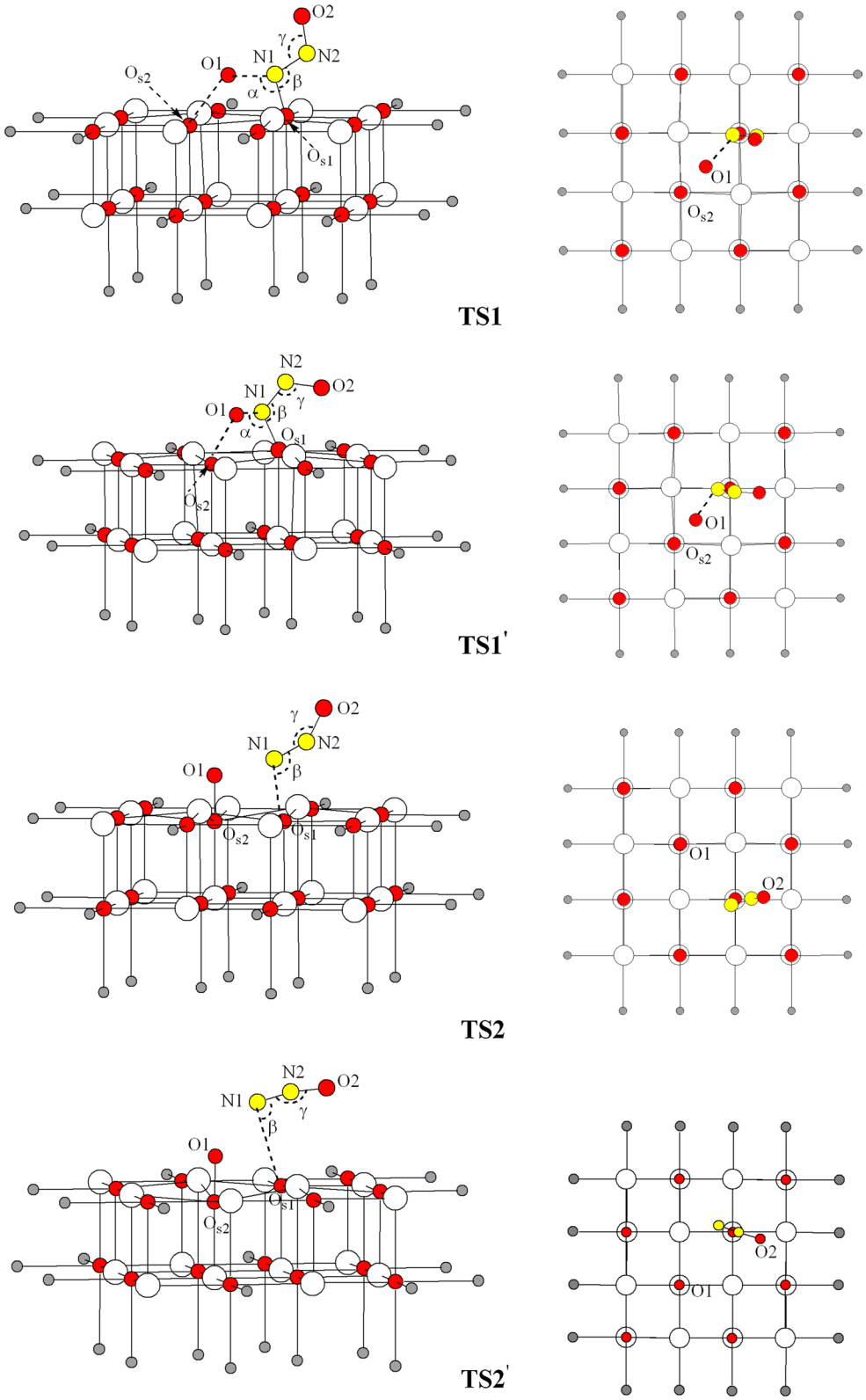

Fig. 4 Optimized transition state (TS) structures on the terrace sites of BaO (*left*, *side view*; *right*, *top view*): TS1 and TS1′ correspond to the dissociation of *cis*-$N_2O_3^{2-}$ and *trans*-$N_2O_3^{2-}$, respectively, to form *cis*-$N_2O_2^{2-}$ and *trans*-$N_2O_2^{2-}$; TS2 and TS2′ correspond to the dissociation of *cis*-$N_2O_2^{2-}$ and *trans*-$N_2O_2^{2-}$, respectively, to form physisorbed N_2O. *Color codes*: *yellow spheres* for N, *red spheres* for O, *large white spheres* for Ba and *small gray spheres* for TIPs. Geometric details may be found in supporting information (SI)

The calculated N–N–O asymmetric stretching mode in **4** appears at 1,884 cm^{-1} on the terrace sites, 1,756 cm^{-1} on the edge sites, and 1,570 cm^{-1} on the corner sites, which are comparable to the experimental band observed around 1,780 cm^{-1} for NO adsorbed on BaO/Y_2O_3 [35]. On the other hand, the calculated N–N–O asymmetric vibration

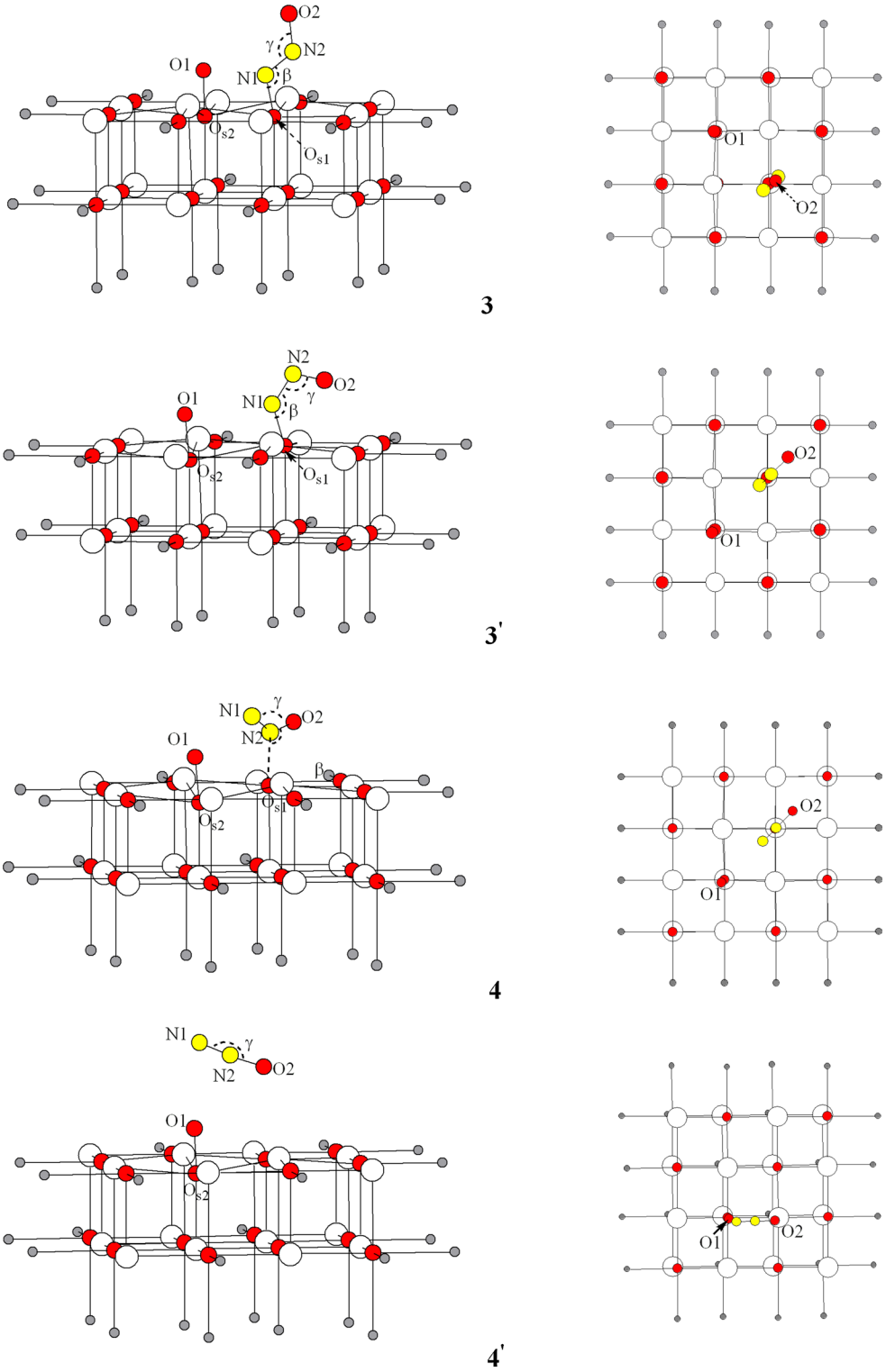

Fig. 5 Optimized structures on the terrace sites of BaO (*left*, *side view*; *right*, *top view*): **3** and **3′** correspond to *trans*-$N_2O_2^{2-}$ and *cis*-$N_2O_2^{2-}$, respectively, plus a surface O_2^{2-} species. **4** and **4′** correspond to a physically adsorbed N_2O plus a surface O_2^{2-} species. *Color codes*: *yellow spheres* for N, *red spheres* for O, *large white spheres* for Ba and *small gray spheres* for TIPs. Geometric details may be found in supporting information (SI)

Table 4 Reaction enthalpy changes and intrinsic activation barriers (kcal/mol) for reaction paths defined in Scheme 1

	ΔH_1	ΔH_2	$H_1^{\ddagger}$	ΔH_3	$H_2^{\ddagger}$	ΔH_4	ΔH_5	$\Delta H_2'$	$H_1^{\ddagger\prime}$	$\Delta H_3'$	$H_2^{\ddagger\prime}$	$\Delta H_4'$	$\Delta H_5'$
Terrace	−28.4	−13.0	52.8	−12.5	25.0	10.2	−0.6	−12.6	47.7	−14.8	7.7	6.1	5.5
Edge	−38.8	−19.5	54.8	−2.7	28.1	2.0	16.6	−29.7	58.3	−5.7	22.9	–	5.6
Corner	−46.1	−43.6	62.1	9.1	45.1	5.7	33.8	−43.8	59.9	1.7	36.7	–	5.2

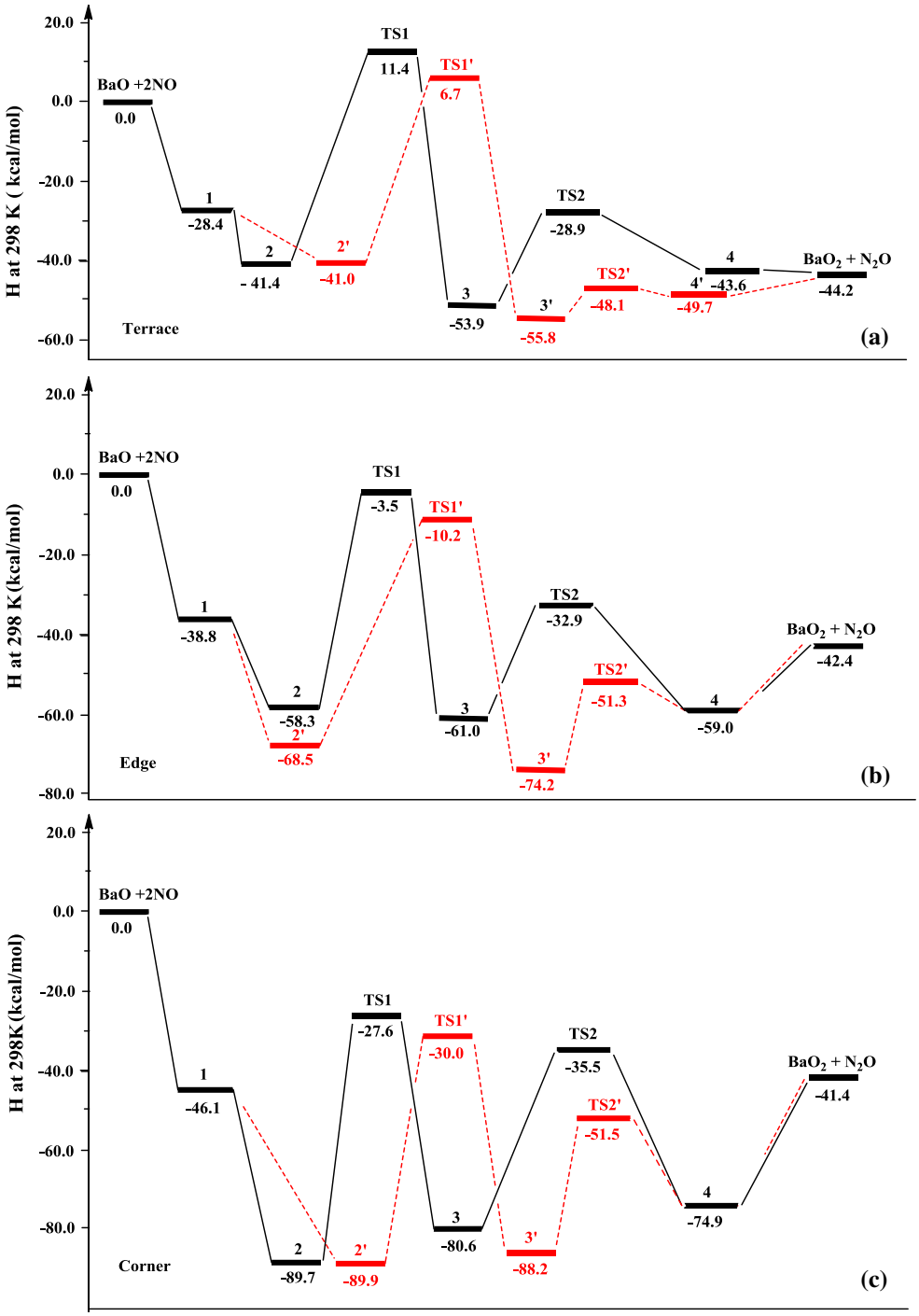

Fig. 6 Energy profiles for NO adsorption and transformations on the **a** terrace **b** edge and **c** corner sites of BaO surfaces. The reaction schemes are defined in Scheme 1. The profiles bifurcate at the formation of *cis*- and *trans*-$N_2O_3^{2-}$ (**2** and **2′**, respectively) species

frequency in **4′** is around 2,377 cm^{-1} on the terrace. This is in good agreement with the experimentally observed band at 2,350 cm^{-1} for the NO/BaO/Y_2O_3 system [35] and is also close to that in the free N_2O [81]. All in all, our calculations support that the peaks around 1,780 and 2,350 cm^{-1} are from N_2O, in accordance with the assignments reported by Ishihara et al. [35] for the NO/BaO/Y_2O_3 systems.

It is particularly interesting to compare the calculated N–N stretching spectra in $N_2O_2^{2-}$ with those observed in experiments for the NSR systems [13, 15]. In fact, the calculated bands are around 1,279 and 1,380 cm^{-1}, which compare fairly well with the bands centered at 1,310 and 1,375 cm^{-1} as observed by Prinetto et al. [13] and 1,380 cm^{-1} as observed by Sedlmair et al. [15], which were assigned to the $N_2O_2^{2-}$ species. Hence, our calculations support that the surface $N_2O_2^{2-}$ will also contribute to the strong peaks observed around 1,310–1,380 cm^{-1} if the barriers from **TS1** (**TS1′**) can be effectively overcome.

4 Concluding remarks

It is commonly reported that conversion of NO to NO_2 over noble metals is required for NO_x storage, while NO reduction also occurs over noble metals [6–10]. Due to the complexity of the NSR system, however, the understanding of the single role of BaO is still incomplete. Some reports suggested that BaO is inactive toward NO [10, 23], while some others showed that NO trapping is already significant on BaO alone [11, 12]. The present work presents a theoretic study on NO adsorption and reaction on BaO, trying to clarify this issue.

The XPS experiments by Schmitz and Baird have highlighted the importance of BaO [12]. Considering that NO_x in exhaust gas is primarily NO and that the surface area of the oxides far exceeds that of the dispersed noble metals, they proposed a unique mechanism that the initial trapping is dominated by the molecular adsorption of NO on BaO to form a nitrite-like (NO_2^-) ad-species [12]. Our calculations support this view of molecular adsorption of NO on BaO, although we are inclined to favor the picture that NO adsorbs on the surface anion sites to form NO_2^{2-}, which is in agreement with the results from the EPR study of NO on the low-coordination sites on MgO and CaO surfaces [78, 79].

A key theoretical concept in understanding the interaction between NO_x and the basic metal oxides is a pairwise, cooperative adsorption mechanism [36], which is shown not to be effective for the (NO, NO) pair on BaO. At high NO pressure, dimerization is favored, in particular, on the low-coordination anion sites to form $N_2O_3^{2-}$. Although the surface $N_2O_2^{2-}$ species is a commonly assumed key intermediate in the NSR system, our calculations suggest that it has to surmount an intrinsic barrier of 50 kcal/mol for its formation. Notably, the high basicity of the low-coordination anion sites on BaO will bring the corresponding transition states below the entrance level, which shall facilitate the $N_2O_2^{2-}$ formation.

Our calculations show that if this barrier can be overcome, the transformation from the surface $N_2O_2^{2-}$ species to N_2O is facile. Indeed, the formation of N_2O has been observed in some NSR and related systems [10, 25, 29, 33, 35]. It is well known that N_2O can be further reduced to N_2 on the metal oxide surfaces [82], which has been characterized with embedded cluster models for BaO(100) [83]. Hence, it is envisioned that BaO not only plays a role in NO storage, but also affects in a way the NO reduction.

The net reaction studied in the present work may be summarized as

$$2\,NO + O^{2-}_{(s)} \longrightarrow N_2O + O^{2-}_{2\,(s)} \qquad (11)$$

It would be anticipated that the surface peroxide species may, in turn, serve as an active oxidant for further NO storage to form NO_2^- and NO_3^- [13, 15, 21, 31, 40], which deserves a detailed investigation.

Some calculated vibrational frequencies of the intermediates are summarized in Table 3, which shall be helpful to assign the bands observed in the experiments. In Table 3, we have also listed the experimental results for the corresponding free molecules (NO and N_2O) and ions (NO_2^-, NO_3^-, $N_2O_3^{2-}$ and $N_2O_2^{2-}$) in compounds [80]. These are the reference numbers with which the IR spectra for surface species in the NSR systems are compared [84]. One has to note that coordination on surfaces will change the peak positions dramatically and the bands from various $N_xO_y^{\delta}$ species overlap. All of these have made the assignment of the corresponding vibrational spectra complicated and controversial. Indeed, the surface NO_2^{2-} and $N_2O_3^{2-}$ species provide an alternative explanation of the experimentally observed IR spectra which were previously assigned to the nitrite/nitrate and hyponitrite species [13, 15].

Further investigation is necessary to see how different reactant gases adsorb, react and even compete against each other for a specific active site, and how the interplay between different components in a real NSR catalyst will change the energy profiles or even change the reaction mechanisms.

Acknowledgments This work was supported by the Ministry of Science and Technology (2013CB834606, 2011CB808505), National Natural Science Foundation of China (21133004), and the Natural Science Foundation of Shandong Province (ZR2010BM041), China.

References

1. Epling WS, Campbell LE, Yezerets A, Currier NW, Parks JE II (2004) Overview of the fundamental reactions and degradation mechanisms of NOx storage/reduction catalysts. Catal Rev Sci Eng 46:163–245
2. Liu ZM, Woo SI (2006) Recent advances in catalytic DeNOx science and technology. Catal Rev Sci Eng 48:43–89
3. Roy S, Baiker A (2009) NOx storage–reduction catalysis: from mechanism and materials properties to storage–reduction performance. Chem Rev 109:4054–4091
4. Granger P, Parvulescu VI (2011) Catalytic NOx abatement systems for mobile sources: from three-way to lean burn after-treatment technologies. Chem Rev 111:3155–3207
5. Szanyi J, Yi CW, Mudiyanselage K, Kwak JH (2013) Understanding automotive exhaust catalysts using a surface science approach: model NOx storage materials. Top Catal 56:1420–1440
6. Takahashi N, Shinjoh H, Iijima T, Suzuki T, Yamazaki K, Yokota K, Suzuki H, Miyoshi N, Matsumoto S, Tanizawa T, Tanaka T, Tateishi S, Kasahara K (1996) The new concept 3-way catalyst for automotive lean-burn engine: NOx storage and reduction catalyst. Catal Today 27:63–69
7. Matsumoto S (1996) DeNOx catalyst for automotive lean-burn engine. Catal Today 29:43–45
8. Bögner W, Krämer M, Krutzsch B, Pischinger S, Voigtländer D, Wenninger G, Wirbeleit F, Brogan MS, Brisley J, Webster DE (1995) Removal of nitrogen oxides from the exhaust of a lean-tune gasoline engine. Appl Catal B Environ 7:153–171

9. Lietti L, Forzatti P, Nova I, Tronconi E (2001) NOx storage reduction over Pt-Ba/γ–Al_2O_3 catalyst. J Catal 204:175–191
10. Fridell E, Skoglundh M, Westerberg B, Johansson S, Smedler G (1999) NOx storage in barium-containing catalysts. J Catal 183:196–209
11. Muncrief RL, Khanna P, Kabin KS, Harold MP (2004) Mechanistic and kinetic studies of NOx storage and reduction on Pt/BaO/Al_2O_3. Catal Today 98:393–402
12. Schmitz PJ, Baird RJ (2002) NO and NO_2 adsorption on barium oxide: model study of the trapping stage of NOx conversion via lean NOx traps. J Phys Chem B 106:4172–4180
13. Prinetto F, Ghiotti G, Nova I, Lietti L, Tronconi E, Forzatti P (2001) FT-IR and TPD investigation of the NOx storage properties of BaO/Al_2O_3 and Pt-BaO/Al_2O_3 catalysts. J Phys Chem B 105:12732–12745
14. Fridell E, Persson H, Olsson L, Westerberg B, Amberntsson A, Skoglundh M (2001) Model studies of NOx storage and sulphur deactivation of NOx storage catalyst. Top Catal 16(17): 133–137
15. Sedlmair C, Seshan K, Jentys A, Lercher JA (2003) Elementary steps of NOx adsorption and surface reaction on a commercial storage–reduction catalyst. J Catal 214:308–316
16. Fridell E, Persson H, Westerberg B, Olsson L, Skoglundh M (2000) The mechanism for NOx storage. Catal Lett 66:71–74
17. Westerberg B, Fridell E (2001) A transient FTIR study of species formed during NOx storage in the Pt/BaO/Al_2O_3 system. J Mol Catal A Chem 165:249–263
18. Olsson L, Persson H, Fridell E, Skoglundh M, Andersson B (2001) A kinetic study of NO oxidation and NOx storage on Pt/Al_2O_3 and Pt/BaO/Al_2O_3. J Phys Chem B 105:6895–6906
19. Mahzoul H, Brilhac JF, Gilot P (1999) Experimental and mechanistic study of NOx adsorption over NOx trap catalysts. Appl Catal B Environ 20:47–55
20. Su Y, Amiridis MD (2004) In situ FTIR studies of the mechanism of NOx storage and reduction on Pt/Ba/Al_2O_3 catalysts. Catal Today 96:31–41
21. Kabin KS, Khanna P, Muncrief RL, Medhekar W, Harold MP (2006) Monolith and TAP reactor studies of NOx storage on Pt/BaO/Al_2O_3: elucidating the mechanistic pathways and roles of Pt. Catal Today 114:72–85
22. Desikusumastuti A, Happel M, Dumbuya K, Staudt T, Laurin M, Gottfried JM, Steinrück H-P, Libuda J (2008) Modeling NOx storage materials: on the formation of surface nitrites and nitrates and their identification by vibrational spectroscopy. J Phys Chem C 112:6477–6486
23. Tsami A, Grillo F, Bowker M, Nix RM (2006) Model NSR catalysts: fabrication and reactivity of barium oxide layers on Cu(111). Surf Sci 600:3403–3418
24. Szanyi J, Kwak JH, Hanson J, Wang C, Szailer T, Peden CHF (2005) Changing Morphology of BaO/Al_2O_3 during NO_2 Uptake and Release. J Phys Chem B 109:7339–7344
25. Hess C, Lunsford JH (2002) Mechanism for NO_2 storage in barium oxide supported on magnesium oxides studies by in situ Raman spectroscopy. J Phys Chem B 106:6358–6360
26. Chi Y, Chuang SSC (2003) Infrared and TPD studies of nitrates adsorbed on Tb_4O_7, La_2O_3, BaO, and MgO/γ–Al_2O_3. J Phys Chem B 107:1982–1987
27. Cheng L, Ge Q (2008) Effect of BaO morphology on NOx abatement: NO_2 interaction with Unsupported and γ–Al_2O_3-supported BaO. J Phys Chem C 112:16924–16931
28. Cheng L, Ge Q (2007) Effect of γ–Al_2O_3 substrate on NO_2 interaction with supported BaO clusters. Surf Sci 601:L65–L68
29. Burch R, Fornasiero P, Watling TC (1998) Kinetics and mechanism of the reduction of NO by n-Octane over Pt/Al_2O_3 under lean-burn conditions. J Catal 176:204–214
30. Broqvist P, Gronbeck H, Fridell E (2004) Characterization of NOx species adsorbed on BaO: experiment and theory. J Phys Chem B 108:3523–3530
31. Xie S, Mestl G, Rosynek MP, Lunsford JH (1997) Decomposition of nitric oxide over barium oxide supported on magnesium oxide. 1. Catalytic results and in situ Raman spectroscopic evidence for a barium–nitro intermediate. J Am Chem Soc 119:10186–10191
32. Klingenberg B, Vannice MA (1999) NO adsorption and decomposition on La_2O_3 studied by DRIFTS. Appl Catal B Environ 21:19–33
33. Wang Y, Jacobi K, Ertl G (2003) Interaction of NO with the Stoichiometric RuO_2(110) Surface. J Phys Chem B 107:13918–13924
34. Rodriguez JA, Azad S, Wang L-Q, García J, Etxeberria A, Gonzalez L (2003) Electronic and chemical properties of mixed-metal oxides: adsorption and reaction of NO on SrTiO(100). J Chem Phys 118:6562–6571
35. Ishihara T, Goto K (2011) Direct decomposition of NO over BaO/Y_2O_3 catalyst. Catal Today 164:484–488
36. Schneider WF (2004) Qualitative differences in the adsorption chemistry of acidic (CO_2, SOx) and amphiphilic (NOx) species on the alkaline earth oxides. J Phys Chem B 108:273–282
37. Tutuianu M, Inderwildi OR, Bessler WG, Warnatz J (2006) Competitive adsorption of NO, NO_2, CO_2, and H_2O on BaO(100): a quantum chemical study. J Phys Chem B 110:17484–17492
38. Marta Branda M, Valentin CD, Pacchioni G (2004) NO and NO_2 adsorption on terrace, step, and corner sites of the BaO Surface from DFT Calculations. J Phys Chem B 108:4752–4758
39. Ferullo RM, Fuente SA, Branda MM, Castellani NJ (2007) Theoretical study of N_2O_2 interaction with BaO(1 0 0) surface. J Mol Struct THEOCHEM 818:57–64
40. Zubieta C, Castellani NJ, Ferullo RM (1009) High reactivity of nitric oxide with peroxo groups on BaO particles DFT calculations. Comput Theor Chem 2013:1–7
41. Lu X, Xu X, Wang N, Zhang Q (1999) Adsorption and decomposition of NO on magnesium oxide: a quantum chemical study. J Phys Chem B 103:5657–5664
42. Valentin CD, Pacchioni G, Abbet S, Heiz U (2002) Conversion of NO to N_2O on MgO Thin Films. J Phys Chem B 106:7666–7673
43. Valentin CD, Pacchioni G, Bernasconi M (2006) Ab Initio molecular dynamics simulation of NO reactivity on the CaO(001) Surface. J Phys Chem B 110:8357–8362
44. Pacchioni G, Ricart JM, Illas F (1994) Ab initio cluster model calculations on the chemisorption of CO_2 and SO_2 probe molecules on MgO and CaO (100) Surfaces. A theoretical measure of oxide basicity. J Am Chem Soc 116:10152–10158
45. Beck AD (1988) Density-functional exchange-energy approximation with correct asymptotic behavior. Phys Rev A 38:3098–3100
46. Becke AD (1993) Density functional thermochemistry. III. The role of exact exchange. J Chem Phys 98:5648–5652
47. Slater JC (1974) Quantum theory of molecules and solids, vol 4. McGraw-Hill, New York
48. Vosko SH, Wilk L, Nusair M (1980) Accurate spin-dependent electron liquid correlation energies for local spin density calculations: a critical analysis. Can J Phys 58:1200–1211
49. Stephens PJ, Devlin FJ, Chabalowski CF, Frisch MJ (1994) Ab initio calculation of vibrational absorption and circular dichroism spectra using density functional force fields. J Phys Chem 98:11623–11627
50. Lee C, Yang W, Parr RG (1988) Development of the Colle–Salvetti correlation-energy formula into a functional of the electron density. Phys Rev B 37:785–789
51. Liu W-G, Goddard WA III (2012) First-principles study of the role of interconversion between NO_2, N_2O_4, cis-ONO–NO, and *trans*-ONO–NO in chemical processes. J Am Chem Soc 134:12970–12978

52. Xu X, Lu X, Wang NQ, Zhang QE (1995) Charge-Consistency Modelling of CO/NiO(100) Chemisorption System. Chem Phys Lett 235:541–547
53. Xu X, Lu X, Wang NQ, Zhang QE (2004) Cluster modeling of chemisorption and reactions on metal oxide surfaces. Acta Phys Chim Sin 20:1045–1054
54. Xu X, Nakatsuji H, Lu X, Ehara M, Cai Y, Wang NQ, Zhang QE (1999) On the cluster modeling of metal oxides: case study of MgO and CO/MgO adsorption system. Theor Chem Acc 102:170–179
55. Lu X, Xu X, Wang NQ, Zhang QE, Ehara M, Nakatsuji H (1998) Cluster modeling of metal oxides: how to cut out a cluster? Chem Phys Lett 291:445–452
56. Xu X, Nakatsuji H, Ehara M, Lu X, Wang NQ, Zhang QE (1998) Cluster modeling of metal oxides: the influence of the surrounding point charges on the embedded cluster. Chem Phys Lett 292:282–288
57. Wyckoff RWG (1963) Crystal structures, 2nd edn. Interscience, New York
58. Winter NW, Pitzer RM, Temple DK (1987) Theoretical study of a Cu+ ion impurity in a NaF host. J Chem Phys 86:3549–3556
59. Nygren MA, Petterson LG, Barandiaran Z, Seijo L (1994) Bonding between CO and the MgO(001) surface: a modified picture. J Chem Phys 100:2010–2018
60. Wadt WR, Hay PJ (1985) Ab initio effective core potentials for molecular calculations. Potentials for main group elements Na to Bi. J Chem Phys 82:284–288
61. Wadt WR, Hay PJ (1985) Ab initio effective core potentials for molecular calculations. Potentials for K to Au including the outermost core orbitals. J Chem Phys 82:299–310
62. Frisch MJ et al (2003) Gaussian03. Gaussian Inc., Pittsburgh
63. Hehre WJ, Ditchfield R, Pople JA (1972) Self-consistent molecular-orbital methods. XII. Further extensions of Gaussian-type basis sets for use in molecular-orbital studies of organic molecules. J Chem Phys 56:2257–2261
64. Miletic M, Gland JL, Hass KC, Schneider WF (2003) First-principles characterization of NOx adsorption on MgO. J Phys Chem B 107:157–163
65. Lu N-X, Fu G, Xu X, Wan HL (2008) Mechanisms for O_2 dissociation over the BaO (100) surface. J Chem Phys 128:034702 1–9
66. Grönbeck H, Broqvist P, Panas I (2006) Fundamental aspects of NOx adsorption on BaO. Surf Sci 600:403–408
67. Valentin CD, Figini A, Pacchioni G (2004) Adsorption of NO and NO2 on terrace and step sites and on oxygen vacancies of the CaO(001) Surface. Surf Sci 556:145–158
68. Lu X, Xu X, Wang NQ, Zhang QE (1999) N_2O decomposition on MgO and Li/MgO catalysts: a quantum chemical study. J Phys Chem B 103:3373–3379
69. Lu X, Xu X, Wang NQ, Zhang QE, Ehara M, Nakatsuji H (1999) Heterolytic adsorption of H_2 on ZnO(100) surface: an ab initio SPC cluster model study. J Phys Chem B103:2689–2695
70. Lu X, Xu X, Wang NQ, Zhang QE (2000) Chemisorption-induced oligomerization of CO over strongly basic sites of MgO solid: a hybrid B3LYP study. J Phys Chem B104:10024–10031
71. Fu G, Xu X, Lu X, Wan HL (2005) Mechanisms of initial propane activation on molybdenum oxides: a density functional theory study. J Phys Chem B 109:6416–6421
72. Fu G, Xu X, Lu X, Wan HL (2005) Mechanisms of methane activation and transformation on molybdenum oxide based catalysts. J Am Chem Soc 127:3989–3996
73. Fu G, Xu X, Wan HL (2006) Mechanism of methane oxidation by transition metal oxides: a cluster model study. Catal Today 117:133–137
74. Fu G, Yi XD, Huang CJ, Xu X, Weng WZ, Xia WS, Wan HL (2007) Developing selective oxidation catalysts of light alkanes: from fundamental understanding to rational design. Surf Rev Lett 14:645–656
75. Lu NX, Xu X (2011) Theoretical study of $NO_x/CO_2/H_2O$ adsorption on BaO(001) surface. Acta Chim Sin 69:1264–1268
76. Yuan R-M, Fu G, Xu X, Wan HL (2011) Brønsted-NH4 + mechanism versus nitrite mechanism: new insight into the selective catalytic reduction of NO by NH3. Phys Chem Chem Phys 13:453–460
77. Yuan R-M, Fu G, Xu X, Wan HL (2011) Mechanisms of selective catalytic oxidation (SCO) of ammonia over vanadium oxides. J Phys Chem C 115:21218–21229
78. Lunsford JH (1967) EPR study of NO adsorbed on magnesium oxide. J Chem Phys 46:4347–4351
79. Paganini MC, Chiesa M, Martino P, Giamello E (2002) EPR study of the surface basicity of calcium oxide. 1. The CaO–NO chemistry. J Phys Chem B 106:12531–12536
80. Laane J, Olsen JR (1980) Characterization of nitrogen oxides by vibrational spectroscopy. Prog Inorg Chem 27:465–513
81. Palmer MS, Neurock M (2002) Periodic density functional theory study of the dissociative adsorption of molecular oxygen over La_2O_3. J Phys Chem B 106:6543–6547
82. Kapteijn F, Rodriguez-Mirasol J, Moulijn JA (1996) Heterogeneous catalytic decomposition of nitrous oxide. Appl Catal B Environ 9:25–64
83. Karlsen EJ, Pettersson LGM (2002) N2O decomposition over BaO: including effects of coverage. J Phys Chem B 106:5719–5721
84. Hadjiivanov KI (2000) Identification of Neutral and charged NxOy surface species by IR spectroscopy. Catal Rev Sci Eng 42:71–144